Revista Mexicana de Física S **58** (2) 12–15 DICIEMBRE 2012

Synthesis and characterization of Fe-doped SnO_2

C. Cajas[a], F.H. Aragón[b], C.M. Campo[a], J.A.H. Coaquira[b], and J.E. Rodríguez-Páez[a]
[a]*Grupo CYTEMAC, Departamento de Física – Universidad del Cauca,*
Calle 5 N° 4-70 Popayán – Colombia.
e-mail: patolacajas@hotmail.com
[b]*Núcleo de Física Aplicada, Institute of Physics, University of Brasília,*
Brasília 70910-900 DF, Brazil.

Recibido el 25 de junio de 2010; aceptado el 24 de enero de 2011

Fe-doped SnO_2 nanoparticles doped with 5 and 8 mol% were successfully synthesized by a controlled precipitation method. X-ray diffraction (XRD) patterns are consistent with the rutile-type structure. The XRD patterns of thermal-treated samples were analyzed using the Rietveld refinement method. The results are consistent with both the increase of the crystallite size and the disappearance of the residual strain as the temperature of thermal treatment is increased. Meanwhile transmission electron microscopy images corroborate the crystallite size. The analysis of the magnetic measurements suggests the occurrence of superparamagnetism which coexists with a paramagnetic signal.

Keywords: Nanoparticles; Fe-doped SnO_2; oxide-diluted magnetic semiconductors.

Nanopartículas de SnO_2 dopados con hierro a porcentajes de 5% y 8% en moles, fueron sintetizadas por el método de precipitación controlada. Los patrones de difracción de rayos x muestran que las partículas obtenidas presentan una estructura tipo rutilo. Los patrones de difracción de rayos x de las muestras tratadas térmicamente fueron analizadas usando el método de refinamiento Rietvel, los resultados indican un aumento de tamaño del cristalito y un disminución de la tensión residual, a medida que se incrementa el tratamiento térmico. Mientras tanto las imágenes de microscopía electrónica de transmisión confirman el tamaño de cristalito. El análisis de las medidas magnéticas sugiere la presencia de superparamagnetismo que coexiste con una señal paramagnética.

Descriptores: Nanoparticulas; SnO_2 dopado con Fe; óxidos semiconductores magnéticamente diluidos.

PACS: 61.46.Df; 75.75.Cd; 75.75.-c

1. Introduction

The possibility of using the magnetic properties of gas sensing materials instead of their conventional electrical features has increased the scientific and technological interests in dilute magnetic semiconductor nanosized oxides [1]. This is because, while conventional gas sensors based on nanopowder systems face some challenges in the making of electrical contacts and accurate measurements of the electrical responses, the monitoring of magnetic responses of these nanostructured gas sensing materials show no needs for electrical contacts, somehow simplifying the manufacturing of devices [2].

Tin dioxide (SnO_2) is a wide band-gap ($\sim$3.5 eV) semiconductor and widely studied due to its potential applications as: conventional gas sensor due to its high reactivity with environmental gases [3]; catalyst for hydrocarbons oxidation [4]; transparent electrode [5]; and so forth. The transition metals (TM) doping of SnO_2 has been observed to change its sensitivity, selectivity, and time response with respect to a number of pollutant gases. This can be observed when measuring the electrical response of assembled device [6] or when monitoring systematic variations of magnetic properties [1,2]. However, those magnetic gas sensors still require relatively high temperatures (575 K) to operate, and research on alternative room temperature ferromagnetic materials is of key importance for future low temperature devices.

Reports have indicated room temperature ferromagnetic properties in TM-doped SnO_2 thin films and powders [7,8]. Pulsed laser deposited Fe-doped SnO_2 thin films with Fe content in the range 5% were reported to show room-temperature ferromagnetism (RTFM) [9]. Similarly, pulsed laser deposited Ni-doped SnO_2 thin films ($\sim$8% Ni) grown on different substrates also show room-temperature ferromagnetism [10]. However, RTFM in Fe-doped SnO_2 nanoparticles has not been addressed in details, in special considering its dependence on the Fe content. Here we report the investigation of structural and magnetic properties of Fe-doped SnO_2 nanoparticles.

2. Experimetal

SnO_2 nanoparticles doped with 5 and 8 mol% Fe have been synthesized using the controlled precipitation method. The cation precursor for Sn and Fe used in the preparation were $SnCl_2 \bullet 2H_2O$ and $FeSO_4.7H_2O$, respectively. A solution of deionized water and ethanol in similar proportions has been used as the solvent in order to favor the formation of the cassiterite (SnO_2) phase. The precipitation procedure was accomplished by a steady stirring (100 r.m.p) and monitoring the pH of the solution. After fixing the pH, the solutions of Sn and Fe precursors were mixed and left for 24 h at room temperature. The amount of Fe was controlled according to the relation: Fe/(Fe+Sn). Several washing procedures were made with a dietilamine (0.1 M) solution after 24 h in order to eliminate the remaining chlorides and/or sulfates in the system. The final powder was thermal treated for 24 h

at 100°C to guarantee the particle size stabilization and thermodynamic equilibrium of the dopant distribution.

The crystalline quality and particle size were determined from X-ray powder diffraction (XRD) measurements using Cu-$K\alpha$ radiation using a Bruker diffractometer, model D8 advanced. The analysis of XRD patterns were carried out using the Rietveld method (DBWS program). XRD data were corroborated with Transmission Electron Microscopy (TEM) experiments. Magnetic measurements in the temperature range of 5 to 300 K and in applied magnetic fields up to 90 kOe were carried out using a VSM magnetometer (Quantum Design, PPMS).

3. Results and discussion

3.1. Structural characterization

In Fig. 1 is shown the XRD diffraction patterns of the sample Fe-doped SnO_2 with 8 mol% and pH=8 after a thermal treatment. All patterns show Bragg reflections which are consistent with a rutile-type structure (space group, $P4_2mnm$). The absence of additional reflections indicates that the Fe ions are incorporated in the crystalline structure likely substituting Sn ions. This finding is supported by the observation of a local vibration mode in Raman spectra which is assigned to Fe ions located in Sn sites (not shown here). The increase in the temperature of treatment drives to peaks narrowing without the rising of additional reflections which warrant the stability

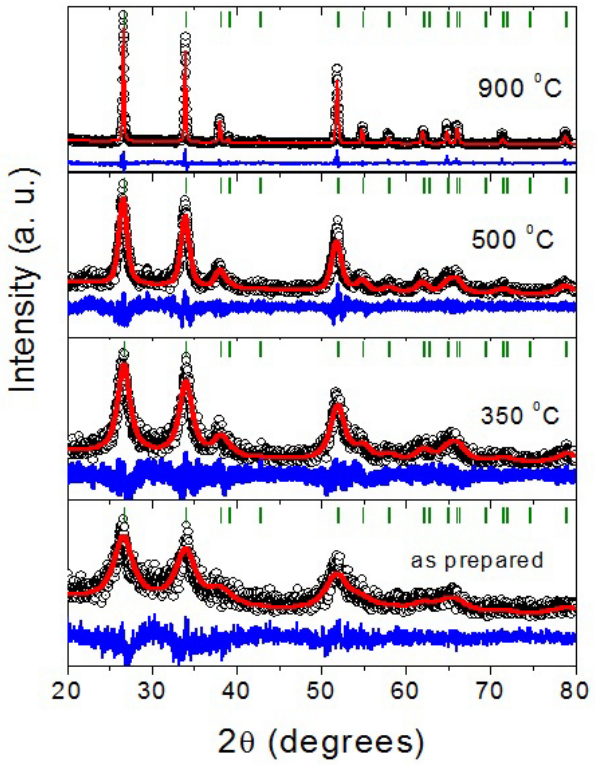

FIGURE 1. XRD patterns of the Fe-doped SnO_2 with 8 mol% (pH=8). The thermal treatments were carried out for 1h in the temperatures showed in each plot.

TABLE I. Parameters obtained from the Rietveld refinement of Fe-doped SnO_2 nanoparticles doped with 8 mol% (pH=8). $\langle D\rangle$ is the crystallite size, $\langle\varepsilon\rangle$ is the estimated strain, c/a is the ratio of the lattice parameters, R_{wp} and R_B are the refinement indexes. Numbers between parentheses represent the uncertainties.

Temp. (°C)	$\langle D\rangle$ (nm)	$\langle\varepsilon\rangle$ (%)	c/a	$R_{wp}/R_{\rm exp}$	R_B (%)
as prepared	3(1)	0.754(2)	0.671	1.2	6.08
350	4(1)	0.581(2)	0.672	0.7	6.28
500	13(1)	0.411(2)	0.671	1.1	5.95
900	52(1)	0.072(2)	0.672	0.5	6.16

of the rutile-type phase and exclude to possible formation of additional phases.

A peak narrowing can be attributed to a crystallite size growing. However, it is known that a variation of the linewidth (full width at half maximum) could be also related to the occurrence of lattice strain and an adequate analysis must be obtained by taking into account the effect of a residual strain and the crystallite size variation. In order to evaluate those contributions, the whole set of Bragg reflections were refined using the Rietveld method. The peak shape was modelled using the Thompson-Cox-Hastings pseudo-Voigt function (TCH-pV) given by [11]:

$$TCH - pV = \eta L + (1-\eta)G, \tag{1}$$

where L and G represent the Lorentzian and Gaussian peak function, respectively, and η is a mixing parameter. The solid red lines in Fig. 1 represent the refinements.

The linewidht for the Gaussian and Lorentzian contributions are given by

$$H_G^2 = U\tan^2\theta + V\tan\theta + W + \frac{Z}{\cos^2\theta},$$

and

$$H_L^= X\tan\theta + \frac{Y}{\cos^\theta},$$

respectively, where U, V, W, Z, X e Y are refined parameters. During the refinement process, only the parameters U, Z, X and Y, which are related with the crystalline size and residual strain were refined. Those parameters were corrected from the instrumental contribution by subtracting the values obtained from the refinement of the XRD pattern of a standard sample (Si single crystal).

The mean crystallite size, $\langle$D$\rangle$ and the $\langle\varepsilon\rangle$ can be estimated using the linewidths and the relations reported in Ref. 11. In Table I are shown the values of $\langle$D$\rangle$, $\langle\varepsilon\rangle$, the lattice-parameters ratio and the parameters of the fit quality for some temperatures of thermal treatment

The crystallite size shows a clear increasing tendency as the temperature of the thermal treatment (TT) is increased. This result is in agreement with that reported in the literature [12]. The unit cell volume and the c/a ratio do not show

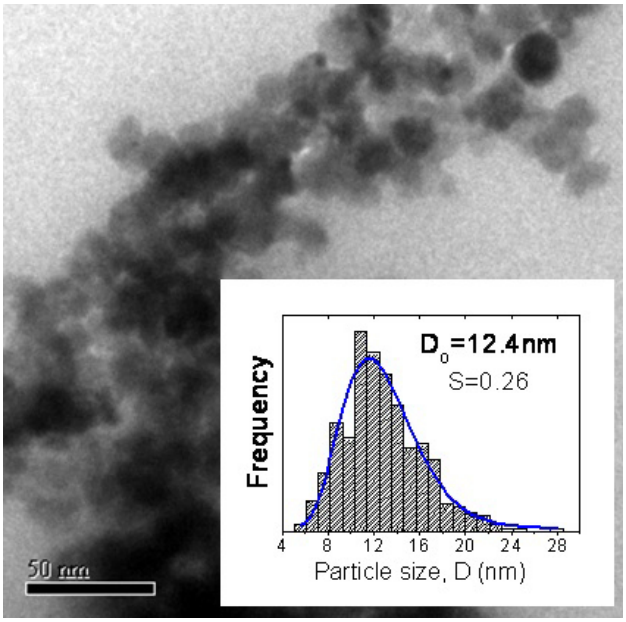

FIGURE 2. TEM image obtained for the Fe-doped SnO_2 nanoparticles with 8 mol% Fe (pH=8). In the inset is shown the histogram mounted as described in the text and modeled by the log-normal function.

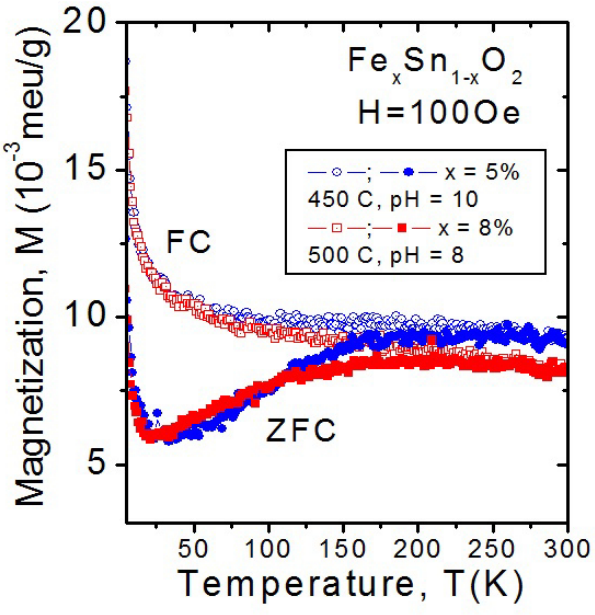

FIGURE 3. Zero-field-cooled (ZFC) and field-cooled (FC) curves as a function of the temperature (T) obtained at H=100 Oe for the Fe-doped SnO_2 nanoparticles.

any tendency as TT is increased which suggests that the crystallite growth is isotropic and that the Fe ions do not outgo from the crystalline structure. However, the residual strain shows a progressive decrease as TT is increased or when the crystallite size grows. It is known that in low-dimensional systems such as nanoparticles, it is expected to have a shell of disordered states stabilized by the translational symmetry breaking and the reduced coordination of surface atoms. An estimative of the shell thickness is found to be d$\sim$1 nm for 10 nm-sized nanoparticles and this thickness becomes larger when the particle size is reduced [13]. The relatively large residual strain estimated for the as prepared sample (3 nm in size) must be related with its larger surface/volume ratio. But, when the surface/volume ratio (larger particles) becomes smaller, the residual strain should become negligible. The residual strain must be related to the Raman modes likely activated by disordered states induced by the residual strain at the particles surface (results not shown here).

3.2. Microscopy study

In order to further corroborate the XRD results, measurements of Transmission Electron Microscopy (TEM) were carried out. In Fig. 2 is shown a TEM image obtained for the sample with 8 mol% Fe (pH=8) thermal-treated at 500°C. Several images were used to count n=673 particle size using the program Image-Pro. A histogram of the particle sizes was mounted using the Sturges method [14]. The bin-width (W) is obtained from: $W = (D_{\max} - D_{\min})/k$, with $k = 1 + 3.322\log(n)$.

In the bottom part of Fig. 2 is show the result. The histogram is well modeled by a log-normal distribution:

$$f(D) = 1/(\sigma.D.\sqrt{2\pi})\exp(-\ln[D/D_0]/2\sigma^2).$$

Here $\ln D_0 = \langle \ln D \rangle$ and σ is the size dispersion. A mean particle size of $\langle D \rangle$=12.8 nm and σ =0.26 are obtained from the fit. If we comparate the particle primary size determined from TEM date with the mean crystallite size determinated from analysis of XRD data, we could indicate the existence of monocristallines nanoparticles.

3.3. Magnetic properties

In Fig. 3 is shown the zero-field-cooled (ZFC) and field-cooled (FC) traces obtained at H=100 Oe for samples with 5 and 8 mol% which were thermal-treated approximately at the same temperature (450 and 500°C). As can be observed, both nanoparticulated samples show features consistent with a magnetic-thermal relaxation process. The ZFC traces show a broad maximum at $\sim$200 K and the irreversibility between ZFC and FC traces starts above the maximum (at $\sim$250 K for the Fe-doped with 8 mol%). The increasing tendency observed in the low-temperature region as the temperature is decreased for both samples must be associated with a paramagnetic contribution coming from extrinsic impurities or extremely small particles or magnetic clusters which are not detected by XRD experiments due to its detection limit.

In order to estimate the effective anisotropy constant, the Arrhenius law is used: $\tau = \tau_0 \exp(K_{\text{eff}} V/k_B T)$, where τ is the relaxation time, τ_0 is the characteristic time ($\sim 10^{-9}$ s), K_{eff} is a effective anisotropy constant and V is the particle volume. By using the mean size determined from XRD data

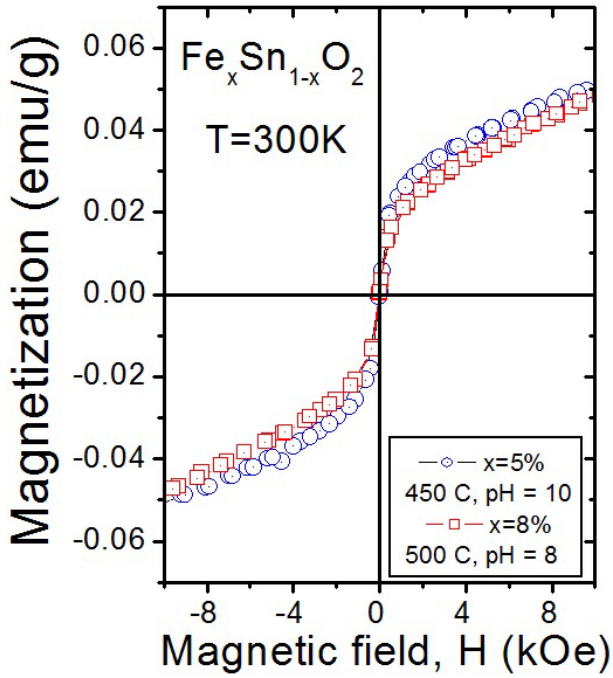

FIGURE 4. Magnetization (M) as a function of the magnetic field (H) obtained at 300 K for the samples indicated in the figure.

and assuming the T_m as the representative temperature for the thermal blocking of the whole system, $K_{\text{eff}} \sim 4\times10^4 \text{J/m}^3$ is obtained for the samples treated at 500°C.

In Fig. 4 is shown the magnetic isotherms (M vs. H) obtained at 300 K for the Fe-doped SnO_2 nanoparticles with 5 and 8 mol%. Even though the absence of coercive field at 300 K, the tendency to saturation of the magnetization observed in the central region (low-field region) suggests the occurrence of particle-particle interactions which seem to survive well-above the blocking temperature. A coercive field H$\sim$70 Oe is determined from the M vs. H curve obtained at T=5 K, although the contribution associated only with the thermally blocked moments is overwhelmed by the stronger paramagnetic contribution coming from extrinsic impurities or paramagnetic regions of the particle. Preliminary room-temperature Mössbauer spectra are consistent with the presence of irons in the valence state Fe^{3+}. Those iron ions are expected to substitute Sn^{4+} ions generating oxygen vacancies in order to keep the charge neutrality. Those oxygen vacancies must play an important role in the magnetic response of the system as determined in Ni-doped SnO_2 nanoparticles synthesized by a polymer precursor method [15]. However, in order to determine the origin of the superparamagnetic behavior and its relation with the particle size and content of dopant, additional characterizations are needed.

4. Conclusions

XRD analyses indicate that the structure of Fe-doped SnO_2 nanoparticles doped up to 8 mol% remain to be a rutile-type. Meanwhile, the thermal treatment does not modify the crystalline structure the mean crystallite size and the residual strain show decreasing tendencies as the temperature of the treatment is increased. That residual strain must be associated with the disordered states occurring at the particle surface which are favored by the translational symmetry breaking. The magnetic response is consistent with the occurrence of superparamagnetism which coexists with a paramagnetic signal.

Acknowledgements

This work was financially supported by the Brazilian agencies CNPq, CAPES and FAP/DF. The authors are grateful to J. A. Dias for his help with the XRD measurements, to Dr. P. de Souza for his help with TEM measurements and to Dr. S. K. Malik for his helpful discussions.

1. A. Punnoose, K.M. Reddy, J. Hays, and A. Thurber, *Appl. Phys. Lett.* **89** (2006) 112509.
2. A. Thurber, K.M. Reddy, and A. Punnoose, *J. Appl. Phys.* **105** (2009) 07E706.
3. B. Bahrami, A. Khodadadi, M. Kazemeini, and Y. Mortazavi, *Sens. Actuators B* **133** (2008) 352.
4. R. Pearce, and W.R. Patterson, "*Catalysis and Chemical Processes*" (Leonard Hill, Glasgow 1981).
5. K.G. Godinho, A. Walsh, and G.W. Watson, *J. Phys. Chem. C* **113** (2009) 439.
6. P. Hidalgo, R.H.R. Castro, A.C.V. Coelho, and D. Gouvêa, *Chem. Mater.* **17** (2005) 4149.
7. S.B. Ogale, *et al.*, *Phys. Rev Lett.* **91** (2003) 077205.
8. A. Hays Punnoose, *J. Appl. Phys.* **97** (2005) 10D321.
9. J.M.D. Coey, A.P. Douvalis, C.B. Fitzgerald, and M. Venkatesan, *Appl. Phys. Lett.* **84** (2004) 1332.
10. H. Kimura, T. Fukumura, M. Kawasaki, K. Inaba, T. Hasegawa, and H. Koinuma, *Appl. Phys. Lett.* **80** (2002) 94.
11. C.O. Paiva-Santos, A.A. Cavalheiro, M.A. Zaghete, M. Cilense, J.A. Varela, M.T. Silva, Y.P. Mascarenhas, *JCPDS-Intern. Centre for Diffraction Data, Adv. X-ray Analysis* **44** (2001) 38.
12. A. Diéguez, A. Romano-Rodríguez, A. Vilà, and J.R. Morante, *J. Appl. Phys.* **90** (2001) 1550.
13. A. Millan, A. Urtizberea, N.J.O. Silva, F. Palacio, V.S. Amaral, E. Snoeck, and V. Serin, *J. Magn. Magn. Mater.* **312** (2007) L5–L9.
14. L.C. Figueiredo, "*Nanoparticulated magnetic systems based on maghemite*", Ph.D. thesis, *Institute of Physics* (University of Brasília, 2009). (unpublished).
15. F.H. Aragón, J.A.H. Coaquira, P. Hidalgo, S.L.M. Brito, D. Gouvêa, and R.H.R. Castro, *J. Non-Crystalline Solids*, accepted (2010).